

# Curvature of the chiral pseudo-critical line in QCD

Claudio Bonati,<sup>\*</sup> Massimo D’Elia,<sup>†</sup> Marco Mariti,<sup>‡</sup> Michele Mesiti,<sup>§</sup> and Francesco Negro<sup>¶</sup>  
*Dipartimento di Fisica dell’Università di Pisa and INFN - Sezione di Pisa,*  
*Largo Pontecorvo 3, I-56127 Pisa, Italy*

Francesco Sanfilippo<sup>\*\*</sup>

*School of Physics and Astronomy, University of Southampton, SO17 1BJ Southampton, United Kingdom*  
 (Dated: March 3, 2022)

We determine the curvature of the pseudo-critical line of strong interactions by means of numerical simulations at imaginary chemical potentials. We consider  $N_f = 2 + 1$  stout improved staggered fermions with physical quark masses and the tree level Symanzik gauge action, and explore two different sets of lattice spacings, corresponding to temporal extensions  $N_t = 6$  and  $N_t = 8$ . Both the renormalized chiral condensate and the renormalized chiral susceptibility are used to locate the transition. The determinations obtained from the two quantities are in good agreement, a preliminary continuum extrapolation yields  $\kappa = 0.013(2)(1)$ . We also investigate the impact of a non-zero strange quark chemical potential and compare our results to previous determinations in the literature, discussing the possible sources of systematic errors affecting the various procedures.

PACS numbers: 12.38.Aw, 11.15.Ha, 12.38.Gc, 12.38.Mh

## I. INTRODUCTION

The presence of a finite temperature transition to a new state of strongly interacting matter, where chiral symmetry is restored and quarks and gluons are deconfined, is a well established fact of Quantum Chromodynamics (QCD). Present evidence from lattice QCD simulations indicates that a rapid change of properties takes place, instead of a genuine phase transition, at a pseudo-critical temperature  $T_c$ , which is around 155 MeV for chiral symmetry restoration [1–5]<sup>1</sup>.

How  $T_c$  changes as a function of various external parameters is a question of great importance, especially for considering QCD predictions in phenomenological contexts where such parameters play a role. An example is the baryon chemical potential,  $\mu_B$ , which enters the description of heavy ion collisions and of some astrophysical objects.

A direct lattice determination of  $T_c$  at  $\mu_B \neq 0$  is presently hindered by the well known sign problem, however various methods have been proposed so far to partially circumvent it and to obtain reliable results in the regime of small  $\mu_B$ . A natural parametrization of  $T_c(\mu_B)$  for small chemical potentials, which exploits the symmetry under charge conjugation at  $\mu_B = 0$  and assumes

analyticity around this point is

$$\frac{T_c(\mu_B)}{T_c} = 1 - \kappa \left( \frac{\mu_B}{T_c} \right)^2 + O(\mu_B^4), \quad (1)$$

where the coefficient  $\kappa$  defines the curvature of the pseudo-critical line  $T_c(\mu_B)$ . The curvature can be obtained in lattice QCD simulations in various ways: by suitable combinations of expectation values computed at  $\mu_B = 0$  (Taylor expansion method [6–9]); by determining the pseudo-critical line for purely imaginary values of  $\mu_B$ , for which numerical simulations are feasible, then fixing the behavior for small and real  $\mu_B$  by analytic continuation [10–20]; by reweighting techniques, in which the oscillating complex behavior is shifted from the path integral measure to the physical observables [21, 22]; by a reconstruction of the canonical partition function [23, 24].

A natural candidate for a comparison with QCD predictions is the chemical freeze-out curve in the  $T - \mu_B$  plane, determined by heavy ion collision experiments, which is obtained so as to describe the particle multiplicities according to a thermal-statistical model [25–30]. Depending on the initial beam energy, different values of  $T$  and  $\mu_B$  are obtained, which are thought to correspond to the conditions of last chemical equilibrium of the thermal medium produced after the collision. In general, one can only assume that chemical freeze-out takes place after re-hadronization, i.e. that the freeze-out curve lies below the pseudo-critical line in the  $T - \mu_B$  plane. However, it is also reasonable to guess that chemical freeze-out is reached shortly after re-hadronization, so that the two lines may lie close to each other. Actually, a comparison with lattice determinations of  $T_c(\mu_B)$  does not show a good agreement. In particular, most determinations of  $\kappa$  turn out be a factor 2-3 smaller than the corresponding curvature of the freeze-out curve [31], even if a recent re-analysis of experimental data, which takes into account inelastic collisions after freeze-out, seems to bring to a

<sup>\*</sup>Electronic address: bonati@df.unipi.it

<sup>†</sup>Electronic address: delia@df.unipi.it

<sup>‡</sup>Electronic address: mariti@df.unipi.it

<sup>§</sup>Electronic address: mesiti@pi.infn.it

<sup>¶</sup>Electronic address: fnegro@pi.infn.it

<sup>\*\*</sup>Electronic address: f.sanfilippo@soton.ac.uk

<sup>1</sup> In the following, however, for the sake of simplicity, we will refer to the rapid change of properties as the “transition”, even if no critical behavior is associated with it.

significant reduction of such a discrepancy [32].

On the side of lattice QCD simulations, a complete control over all possible systematics is also desirable. That requires a proper continuum extrapolation and a comparison among different methods adopted to partially overcome the sign problem. Most determinations available at or around the physical point (i.e. by adopting quark masses tuned so as to yield a physical hadron spectrum) have been obtained by the Taylor expansion method, see Ref. [7] (p4-improved action for staggered quarks) and Refs. [8, 9] (stout-smeared improved action for staggered quarks). A recent determination [20], obtained by the method of analytic continuation and adopting a HISQ/tree action discretization of  $N_f = 2+1$  QCD, has provided a value of the curvature which is somewhat larger with respect to previous lattice determinations.

One would like to fully understand the causes of this discrepancy. Apart from possible systematics lying behind either the Taylor expansion method or analytic continuation, one should consider other standard sources of systematic errors, among which the different possible definitions of  $T_c$ , the approach to the thermodynamical limit (finite size effects), to the continuum limit and to the physical point, and the different setup of chemical potentials,  $\mu_u$ ,  $\mu_d$  and  $\mu_s$ , coupled respectively to the up, down and strange quark numbers. For instance, the choice in Ref. [20] has been to fix them to equal values ( $\mu_u = \mu_d = \mu_s = \mu_B/3$ ), while in previous determinations the choice has typically been  $\mu_u = \mu_d = \mu_B/3$  and  $\mu_s = 0$ , which is thought to better reproduce the thermal medium in accordance with the initial conditions of heavy ion collisions, which correspond to strangeness neutrality.

All that claims for a more systematic investigation. In the present study we will provide a determination of the curvature by the method of analytic continuation, adopting a stout staggered fermions discretization of  $N_f = 2+1$  QCD with physical values of the quark masses, and with the tree level improved Symanzik gauge action. We will consider both the case  $\mu_s = 0$  and  $\mu_s \neq 0$  and will monitor two different physical quantities, namely the renormalized chiral condensate and its susceptibility, in order to locate the pseudo-critical temperature for different values of the chemical potentials. Two different sets of lattice spacings on lines of constant physics will be considered (corresponding to  $N_t = 6$  and  $N_t = 8$ , where  $N_t$  is the temporal extent) in order to estimate ultraviolet (UV) cut-off effects. For  $N_t = 6$  we will consider also different spatial volumes in order to estimate finite size effects.

Various purposes can be accomplished in this way:

1. we will compare determinations of the curvature obtained by different methods but with the same lattice discretization [8];
2. we will compare determinations of the curvature obtained by the same method (analytic continuation) but with different discretizations [20] (HISQ vs stout smeared staggered quarks);
3. we will obtain a first indication about the effects on the critical line of the inclusion of a strange quark chemical potential.

The paper is organized as follows. In Section II we provide some details about the lattice discretization adopted in this study, as well as about the observables chosen to locate  $T_c$  and their renormalization. In Section III we describe the method of analytic continuation, with a focus on the possible differences related to the inclusion (or non inclusion) of a strange chemical potential  $\mu_s$ , which stem from differences in the corresponding phase diagrams at imaginary chemical potentials. In Section IV we present our numerical results, which are compared to previous determinations in Section V, where we also briefly review different methods to determine  $\kappa$  adopted in the literature. Finally, in Section VI, we draw our conclusions.

## II. NUMERICAL SETUP AND OBSERVABLES

For  $N_f = 2+1$  QCD one can consider, in general, three independent chemical potentials,  $\mu_u, \mu_d$  and  $\mu_s$ , coupled respectively to  $N_u, N_d$  and  $N_s$ , i.e. the number of up, down and strange quarks. Different conventions can be adopted, for instance it is usual to make reference to the conserved charges  $B, Q$  and  $S$  (baryon number, electric charge and strangeness) and to the chemical potentials coupled to them,  $\mu_B, \mu_Q$  and  $\mu_S$ . The conserved charges are related to the quark numbers by

$$\begin{aligned} B &= (N_u + N_d + N_s)/3 \\ Q &= (2N_u - N_d - N_s)/3 \\ S &= -N_s \end{aligned} \tag{2}$$

from which the relations between the chemical potentials can be deduced

$$\begin{aligned} \mu_u &= \mu_B/3 + 2\mu_Q/3 \\ \mu_d &= \mu_B/3 - \mu_Q/3 \\ \mu_s &= \mu_B/3 - \mu_Q/3 - \mu_S. \end{aligned} \tag{3}$$

In the following we make reference to the convention in terms of  $\mu_u, \mu_d$  and  $\mu_s$ , and translate to the other convention when necessary (e.g., to extract  $\kappa$  given in Eq. (1)).

We perform lattice simulations of  $N_f = 2 + 1$  QCD in the presence of purely imaginary quark chemical potentials,  $\mu_f = i\mu_{f,I}$ ,  $\mu_{f,I} \in \mathbb{R}$ , with  $f = u, d, s$ . We consider the following euclidean partition function of the

discretized theory:

$$\mathcal{Z} = \int \mathcal{D}U e^{-S_{YM}} \prod_{f=u,d,s} \det \left( M_{st}^f[U, \mu_{f,I}] \right)^{1/4}, \quad (4)$$

$$S_{YM} = -\frac{\beta}{3} \sum_{i,\mu \neq \nu} \left( \frac{5}{6} W_{i;\mu\nu}^{1 \times 1} - \frac{1}{12} W_{i;\mu\nu}^{1 \times 2} \right), \quad (5)$$

$$(M_{st}^f)_{i,j} = am_f \delta_{i,j} + \sum_{\nu=1}^4 \frac{\eta_{i;\nu}}{2} \left[ e^{ia\mu_{f,I} \delta_{\nu,4}} U_{i;\nu}^{(2)} \delta_{i,j-\hat{\nu}} - e^{-ia\mu_{f,I} \delta_{\nu,4}} U_{i-\hat{\nu};\nu}^{(2)\dagger} \delta_{i,j+\hat{\nu}} \right]. \quad (6)$$

The functional integration is performed over the gauge links,  $U \in SU(3)$  and  $S_{YM}$  is the tree level improved Symanzik action introduced in Refs. [33, 34], where  $W_{i;\mu\nu}^{n \times m}$  is the trace of the  $n \times m$  loop constructed from the gauge links along the directions  $\mu, \nu$  departing from the  $i$  site. The staggered Dirac operator  $(M_{st}^f)_{i,j}$  defined in Eq. (6) is built up in terms of the two times stout-smear links  $U_{i;\nu}^{(2)}$ , which are constructed following the procedure described in Ref. [35] and using the isotropic smearing parameters  $\rho_{\mu\nu} = 0.15$  for  $\mu \neq \nu$ . The stout smearing improvement is used in order to reduce the effects of finite lattice spacing and taste symmetry violations (for a comparison between different improved staggered discretizations and their effectiveness in reducing taste violations, see Ref. [36]). For each flavor we introduce the imaginary quark chemical potential in the Dirac operator by multiplying all the temporal links in the forward (backward) direction by  $e^{+ia\mu_{f,I}}$  ( $e^{-ia\mu_{f,I}}$ ): that can be viewed as a rotation by an angle  $\theta_f \equiv aN_t \mu_{f,I} = \mu_{f,I}/T$  of the temporal boundary conditions for the quark flavor  $f$ . For each lattice we have studied 3-4 different values of the imaginary chemical potentials (see Table I). As usual for the staggered fermions simulations, the residual fourth degeneracy of the lattice Dirac operator is removed by using the rooting procedure: possible systematics related to this approach have been discussed in the literature (see, e.g., Ref. [37]) and are shared by the other lattice studies with which we are going to compare [7–9, 20].

We perform simulations at finite temperature around the transition temperature, using lattices with two different temporal extensions,  $N_t = 6, 8$ . At fixed  $N_t$ , the temperature  $T = 1/(aN_t)$  of the system is changed by varying the value of the bare coupling constant  $\beta$ . The bare quark masses  $m_s$  and  $m_l$  are accordingly rescaled with  $\beta$ , in order to move on a line of constant physics, with  $m_\pi \simeq 135$  MeV and  $m_s/m_l = 28.15$ ; this line is determined by a spline interpolation of the values reported in Refs. [38, 39], the complete set of adopted parameters is reported in Appendix A. At fixed  $T$ , the two different values of  $N_t$  correspond to different lattice spacings and permit us to estimate UV cut-off effects.

The chiral condensate of the flavor  $f$  is defined as

$$\langle \bar{\psi}\psi \rangle_f = \frac{T}{V} \frac{\partial \log Z}{\partial m_f}, \quad (7)$$

where  $V$  is the spatial volume. Since in our simulations the two light quarks are degenerate with mass  $m_l \equiv m_u = m_d$ , it is convenient to introduce the light quark condensate:

$$\langle \bar{\psi}\psi \rangle_l = \frac{T}{V} \frac{\partial \log Z}{\partial m_l} = \langle \bar{u}u \rangle + \langle \bar{d}d \rangle, \quad (8)$$

which will be renormalized by adopting the prescription introduced in Ref. [40]:

$$\langle \bar{\psi}\psi \rangle_l^r(T) \equiv \frac{\left[ \langle \bar{\psi}\psi \rangle_l - \frac{2m_l}{m_s} \langle \bar{s}s \rangle \right](T)}{\left[ \langle \bar{\psi}\psi \rangle_l - \frac{2m_l}{m_s} \langle \bar{s}s \rangle \right](T=0)}, \quad (9)$$

where  $m_s$  is the bare strange quark mass.

The light quarks chiral susceptibility is given by ( $M_l$  is the Dirac operator corresponding to a single light flavor)

$$\chi_{\bar{\psi}\psi} = \frac{\partial \langle \bar{\psi}\psi \rangle_l}{\partial m_l} = \chi_{\bar{\psi}\psi}^{disc} + \chi_{\bar{\psi}\psi}^{conn} \quad (10)$$

$$\chi_{\bar{\psi}\psi}^{disc} \equiv \frac{T}{V} \left( \frac{N_l}{4} \right)^2 \left[ \langle (\text{Tr} M_l^{-1})^2 \rangle - \langle \text{Tr} M_l^{-1} \rangle^2 \right] \quad (11)$$

$$\chi_{\bar{\psi}\psi}^{conn} \equiv -\frac{T}{V} \frac{N_l}{4} \langle \text{Tr} M_l^{-2} \rangle. \quad (12)$$

In this expression  $N_l$  is the number of degenerate light quarks, that in our case is fixed to  $N_l = 2$ . Traces are computed by noisy estimators, with 8 random vectors for each flavor. The renormalization of the chiral susceptibility is performed by first subtracting the  $T = 0$  contribution (thus removing the additive renormalization) and then multiplying the result by the square of the bare light quark mass to fix the multiplicative UV divergence [38]:

$$\chi_{\bar{\psi}\psi}^r = m_l^2 \left[ \chi_{\bar{\psi}\psi}(T) - \chi_{\bar{\psi}\psi}(T=0) \right]. \quad (13)$$

All the  $T = 0$  quantities have been measured on a symmetric  $N_t = N_s = 32$  lattice.

The renormalization prescriptions Eqs. (9)-(13) are not the only available choices: other approaches exist in the literature (see e.g. Refs. [7, 8]) and in the following sections we will also investigate the dependence of the results on the different renormalization prescriptions adopted.

### III. ANALYTIC CONTINUATION WITH AND WITHOUT A STRANGE QUARK CHEMICAL POTENTIAL

Both the method of analytic continuation from imaginary chemical potentials and the Taylor expansion approach are based on the assumption that the free energy is analytic, at least in a limited region of small chemical potentials.

As it happens for other thermodynamical quantities, it is possible to make an ansatz for the dependence of the pseudo-critical temperature  $T_c(\mu_u, \mu_d, \mu_s)$  which is valid for small chemical potentials. The symmetries of

the theory constrain the possible form of this dependence. First of all, charge conjugation symmetry imposes that  $T_c$ , as well as the free energy itself, be invariant under a simultaneous sign change of all chemical potentials, thus a Taylor expansion of  $T_c$  must include only monomials of overall even degree in the chemical potentials.

Moreover, in the case of two degenerate flavors, isospin symmetry imposes further constraints. By rewriting the coupling to the chemical potentials of the continuum lagrangian in the more compact form  $\bar{\psi}_f \gamma_0 M_{ff'} \psi_{f'}$ , where  $f, f'$  are flavor indices and  $M$  is a  $2 \times 2$  hermitian matrix, which is usually diagonal, it can be shown that the theory is invariant under isospin rotations  $\psi \rightarrow R\psi$ , combined with  $M \rightarrow RMR^\dagger$ , where  $R$  denotes a generic  $SU(2)$  matrix. The dependence of  $T_c$  on the chemical potentials must satisfy such invariance, that means that it can be function only of invariant quantities of the matrix  $M$ . At the leading quadratic order two independent such quantities exist, which can be chosen to be  $\det(M)$  and  $\text{Tr}(M^\dagger M)$  (or alternatively  $[\text{Tr}(M)]^2$ ). To leading order we thus have (see also Ref. [41]):

$$\begin{aligned} T_c(M) &= T_c(0) - \alpha \text{Tr}(M^\dagger M) - \gamma \det(M) = \\ &= T_c(0) - \alpha(\mu_u^2 + \mu_d^2) - \gamma \mu_u \mu_d. \end{aligned} \quad (14)$$

It is interesting that at this level the requirement of isospin invariance is in fact equivalent to the requirement of symmetry under  $u \leftrightarrow d$  exchange. This is particularly relevant since in the lattice discretization of the partition function, Eq. (4), each quark is treated by means of a separate quartic root of a fermion determinant, so that only the symmetry under  $u \leftrightarrow d$  exchange is strictly true at finite lattice spacing. It has been verified in Ref. [18] that, in the discretized  $N_f = 2$  theory, the mixing term  $\gamma$  is small but non-zero, corresponding to a measurable difference between the curvature in terms of the baryon or the isospin chemical potential. In our  $N_f = 2 + 1$  setup, the generalization of Eq. (14) is simply

$$\begin{aligned} T_c(\mu_u, \mu_d, \mu_s) &= T_c(0) - A(\mu_u^2 + \mu_d^2) - B\mu_s^2 \\ &\quad - C\mu_u\mu_d - D\mu_s(\mu_u + \mu_d) + O(\mu^4). \end{aligned} \quad (15)$$

In this study, we are interested only in two particular setups of chemical potentials. In the first case we set  $\mu_u = \mu_d \equiv \mu_l$  and  $\mu_s = 0$ . That coincides with the setup adopted in most studies (like e.g. in Refs. [7, 8]), which is thought to be close to the situation created in heavy ion collisions, where the initial conditions correspond to strangeness neutrality. In this case the expected parametrization is

$$T_c(\mu_l) = T_c(0) - A'\mu_l^2 + O(\mu_l^4) \quad (16)$$

where  $A' = A + C$ .

In the second case, we set  $\mu_s = \mu_l$ : that permits to estimate the effects of the inclusion of  $\mu_s$  and to compare with some previous studies [19, 20]. In this case the parametrization is

$$T_c(\mu_l) = T_c(0) - (A' + B')\mu_l^2 + O(\mu_l^4) \quad (17)$$

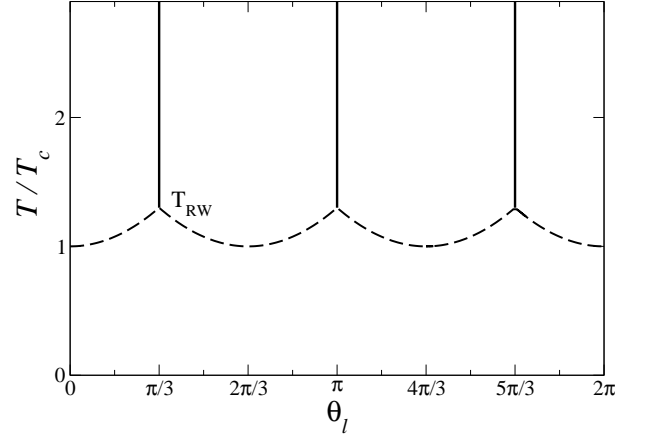


FIG. 1: Sketched phase diagram in the  $T - \theta_l$  plane for  $\mu_s = \mu_l$ . Solid lines indicate the RW lines, while the dashed lines corresponds to the analytic continuation of the pseudo-critical line.

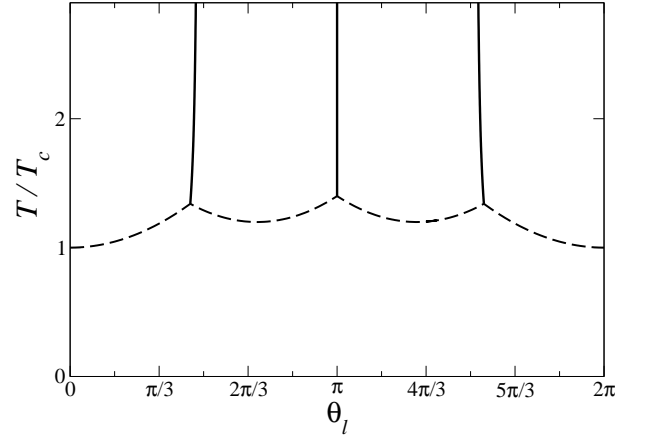


FIG. 2: The same as for Fig. 1, but for  $\mu_s = 0$ . In this case the exact location of the RW-like lines, apart from the one at  $\theta_l = \pi$ , is temperature dependent and known analytically only in the high  $T$  limit.

where  $B' = B + 2D$ . An independent study with  $\mu_u = \mu_d = 0$  and  $\mu_s \neq 0$  would provide direct information on  $B$  and verify if the mixing term  $D$  is negligible or not: this is left for future investigations.

When the chemical potentials are purely imaginary, and if analytic continuation holds true, the following dependence is expected for  $T_c$  as a function of the quantity  $\theta_l = \text{Im}(\mu_l)/T$  introduced in Section II:

$$\frac{T_c(\theta_l)}{T_c(0)} = 1 + R\theta_l^2 + O(\theta_l^4) \quad (18)$$

where  $R = A' T_c(0)$  or  $R = (A' + B') T_c(0)$ , depending on the different setup adopted.

Apart from the possible different values of the curvatures, the fact that  $\mu_s = 0$  or  $\mu_s = \mu_l$  is of course relevant also to non-linear terms in  $\theta_l^2$ , as we are going to discuss in the rest of this section. In this respect, a



substantial difference in the phase diagram in the  $T - \theta_l$  plane may play a significant role. It is well known [42] that when all imaginary chemical potentials are equal, i.e. when the temporal boundary conditions of all quark fields are rotated by the same angle  $\theta_l$ , a translation of  $\theta_l$  by a multiple of  $2\pi/3$  can be cancelled by a center transformation of gauge fields, so that the partition function is periodic in  $\theta_l$  with a period  $2\pi/3$ . Such a periodicity is smoothly realized at low  $T$  [10, 11, 43], while in the high  $T$  regime it is enforced by first order transitions [42], known as Roberge-Weiss (RW) transitions, which are connected with center symmetry and with the dynamics of the Polyakov loop, as explained in more details in the following.

In absence of dynamical fermions, the theory is invariant under center transformations, i.e. gauge transformations which are periodic in time up to a center phase  $\exp(i2\pi k/3)$ , where  $k$  is an integer. However, the trace of the Wilson line in the time direction (Polyakov loop) is not invariant under such transformations. A non-zero expectation value of the Polyakov loop signals the spontaneous breaking of center symmetry at high  $T$ , where the free energy develops three degenerate minima, corresponding to a Polyakov loop oriented along the three different roots of unity  $\exp(2\pi i k/3)$ ,  $k = 0, 1, 2$ . The fermion determinant breaks center symmetry explicitly: for zero imaginary chemical potential its effect is like adding an external magnetic field in a three-dimensional Potts model, aligning the Polyakov loop along the positive real axis in the complex plane, i.e. along  $k = 0$  (see e.g. [44]). An imaginary chemical potential coupled to quark flavor  $f$ , by rotating the temporal boundary conditions in the fermion determinant, rotates the coupling to the Polyakov loop by an angle  $-\theta_f = -\text{Im}(\mu_f)/T$ .

In the high  $T$  phase, if all imaginary chemical potentials are set equal, the Polyakov loop undergoes an abrupt change of orientation, corresponding to the RW transitions, as  $\theta_l$  crosses  $\pi/3$  or odd multiples of it. For such values, the effective magnetic-like coupling to the Polyakov field points exactly in-between two cubic roots of unity, thus leaving an exact residual  $Z_2$  center symmetry, which is spontaneously broken at high  $T$ . The onset of this spontaneous breaking, taking place at the endpoint of the RW line, or RW endpoint, has been the subject of various studies (for a collection of lattice investigations, see Refs. [45–52]).

The presence of the RW transitions places a limitation on the region of imaginary chemical potentials available to analytic continuation: for high  $T$ , only chemical potentials such that  $\theta_l < \pi/3$  can be used to investigate the dependence of the free energy for small values of  $\mu_l$ , since for  $\theta_l > \pi/3$  one is exploring a different analyticity sheet of the free energy, corresponding to a different center sector, even if with identical and periodically repeated physical properties. The pseudo-critical line itself, in particular, develops a non-analyticity at  $\theta_l = \pi/3$ : numerical evidence is that it touches the RW endpoint, where it forms a cusp, and then repeats periodically;

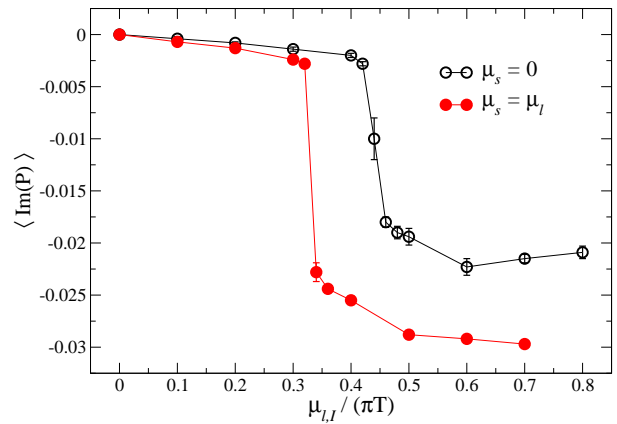


FIG. 3: Imaginary part of the Polyakov loop as a function of  $\theta_l$  at fixed  $T \approx 208$  MeV for  $\mu_s = \mu_l$  and for  $\mu_s = 0$ .

such a situation is depicted schematically in Fig. 1.

When one adopts the setup in which  $\mu_d = \mu_u \equiv \mu_l \neq 0$  and  $\mu_s = 0$ , the phase diagram in the  $T - \theta_l$  plane looks different. The strange quark determinant is independent of  $\theta_l$  and that breaks the  $\pi/3$  periodicity in  $\theta_l$ . In particular, as  $\theta_l$  is increased, the effective coupling of the up and down quark determinants to the Polyakov loop will rotate by an angle  $-\theta_l$ , while that of the strange quark will stay oriented along the positive real axis. As a consequence, the critical value of  $\theta_l$  at which, in the high  $T$  regime, the Polyakov loop jumps from one sector to the other, will be higher than  $\pi/3$ . Given the residual  $2\pi$  periodicity in  $\theta_l$  and the symmetry under inversion of  $\theta_l$ , the expected phase diagram is depicted schematically in Fig. 2: we still have RW-like transition lines at high  $T$ , which however take place for different values of  $\theta_l$  (apart from the one at  $\theta_l = \pi$ ) and separate sectors of the theory which are not equivalent to each other.

We have verified this expectation explicitly by monitoring the Polyakov loop as a function of  $\theta_l$  in the two different setups: results are reported in Fig. 3, where we plot the imaginary part of the Polyakov loop (which jumps when the boundary between two different center sectors is crossed) as a function of  $\theta_l$ . While for  $\mu_s = \mu_l$  the jump takes place at  $\theta_l = \pi/3$ , as expected, when  $\mu_s = 0$  the jump moves forward and takes place approximately at  $\theta_l \simeq 0.45\pi$ . A perturbative computation in the regime of asymptotically high temperatures, performed making use of the one loop effective potential for the Polyakov loop in the presence of massless quarks, gives  $\theta_c \approx 0.482933\pi$ , see Appendix C.

One important consequence is that, for high  $T$ , the region available for analytic continuation is larger for  $\mu_s = 0$  than for  $\mu_s = \mu_l$ : that means that a better control on systematic effects can be attained. Since analytic continuation is actually performed in terms of  $\theta_l^2$ , going from  $\pi/3$  to approximately  $0.45\pi$  means that the available region is almost doubled, i.e. the increase is substantial. Moreover, one may expect that for  $\mu_s = 0$  the possible effects of the critical behavior around the

RW endpoint on the region of small chemical potentials should be milder, since the endpoint is moved further inside the  $T - \theta_l$  plane: such effects include the possible non-linear contributions in  $\theta_l^2$  to the pseudo-critical line  $T_c(\theta_l)$ . This point will be discussed further in Section IV.

#### IV. NUMERICAL RESULTS

We performed simulations for different values of the chemical potentials and  $\mathcal{O}(10)$  temperatures around  $T_c(\mu)$ , on four different lattice sizes:  $16^3 \times 6$ ,  $24^3 \times 6$ ,  $32^3 \times 6$  and  $32^3 \times 8$ . We mainly considered the  $\mu_s = 0$  setup, for the  $32^3 \times 8$  lattice we also studied the case  $\mu_s = \mu_l$ . The Rational Hybrid Monte-Carlo algorithm [53–55] has been used for sampling gauge configurations according to Eq. (4), each single run consisting of 2-5 K trajectories of unit length in molecular dynamics time, with higher statistics around the transition.

To perform the renormalization described in Sec. II, one needs to compute observables also at  $T = 0$  and at the same values of the bare parameters, i.e. at the same UV cutoff. At  $T = 0$  observables depend smoothly on  $\beta$ ; moreover no dependence at all is expected on the imaginary chemical potentials, since they can be viewed as a modification in the temporal boundary conditions which, at  $T = 0$  (hence for ideally infinite temporal extension), are completely irrelevant. For those reasons, we performed a set of simulations on a  $32^4$  lattice, at zero chemical potentials and for a few values of  $\beta$  on the line of constant physics. Then we estimated the observables at intermediate values of  $\beta$  by a suitable interpolation and adopted them to renormalize data at  $T \neq 0$  and generic values of the chemical potentials. More details on the  $T = 0$  measurements are reported in Appendix A.

In Figs. 4 and 5 we plot the results obtained respectively for the renormalized light chiral condensate  $\langle \bar{\psi}\psi \rangle_l^r$  and for the renormalized chiral susceptibility  $\chi_{\bar{\psi}\psi}^r$ , which are our reference observables and have been defined in Eqs. (9)-(13). Since no real phase transition is present in the explored range of chemical potentials, before going on we have to define a prescription to locate the pseudo-critical temperature  $T_c$  (a comparison with the results obtained by other definitions and/or approaches is reported in the next section). We will adopt the two following definitions of  $T_c$ , related to the two different observables studied:

1. the temperature corresponding to the inflection point of the renormalized chiral condensate (as defined by Eq. (9)) ;
2. the temperature corresponding to the maximum of the renormalized chiral susceptibility (as defined by Eq. (13)).

Both these definitions are faithful, *i.e.* when a real phase transition is present its location is correctly identified (in the thermodynamical limit) by means of them.

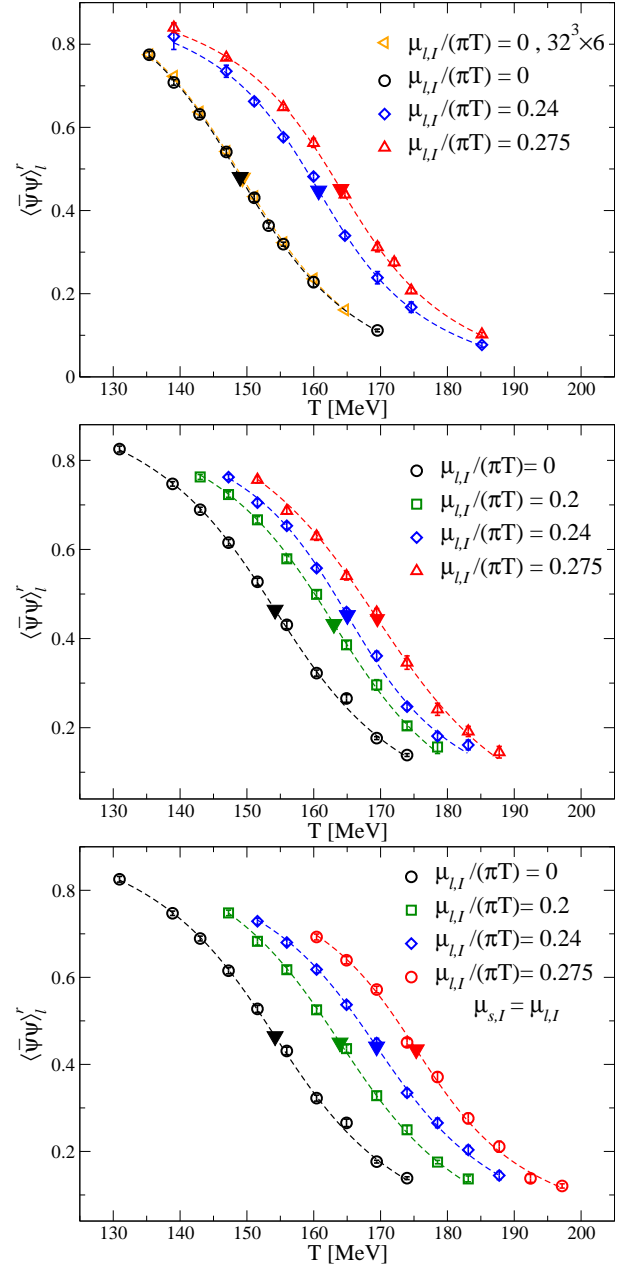


FIG. 4: Renormalized light chiral condensate for various values of  $T$  and  $\mu_l$  respectively on:  $24^3 \times 6$  lattice with  $\mu_s = 0$  (top);  $32^3 \times 8$  lattice with  $\mu_s = 0$  (middle);  $32^3 \times 8$  lattice with  $\mu_s = \mu_l$  (bottom). In the top figure the data from the  $32^3 \times 6$  lattice at  $\mu_l = 0$  are also shown for comparison. Lines correspond to the best fit described in the text and the filled triangles denote the values at the pseudo-critical temperature.

In order to determine the inflection point of the renormalized chiral condensate, we performed a best fit on the data by using the expression

$$\langle \bar{\psi}\psi \rangle_l^r(T) = A_1 + B_1 \arctan(C_1(T - T_c)) , \quad (19)$$

with the four independent parameters  $A_1$ ,  $B_1$ ,  $C_1$  and  $T_c$ . This function is found to well describe the behavior

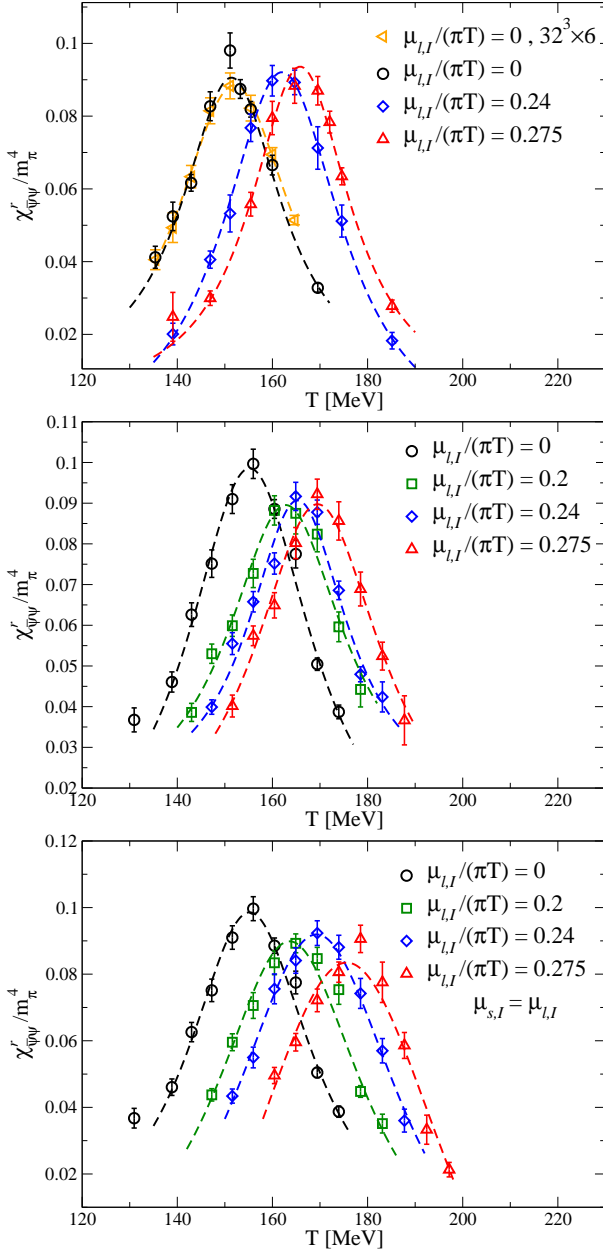


FIG. 5: Renormalized light chiral susceptibility, divided by  $m_\pi^4$ , for various values of  $T$  and  $\mu_l$  respectively on:  $24^3 \times 6$  lattice with  $\mu_s = 0$  (top);  $32^3 \times 8$  lattice with  $\mu_s = 0$  (middle);  $32^3 \times 8$  lattice with  $\mu_s = \mu_l$  (bottom). In the top figure the data from the  $32^3 \times 6$  lattice at  $\mu_l = 0$  are also shown for comparison.

of  $\langle \bar{\psi}\psi \rangle_l^r(T)$  in the whole range of explored temperatures. The best fits obtained by this procedure are plotted, together with the corresponding data points, in Fig. 4, the position of the inflection point being denoted, for each data set, by a filled triangle. The errors on the fit parameters have been estimated by means of a bootstrap analysis; results for  $T_c$  are stable, within the quoted errors, if a different interpolation (e.g., through an hyperbolic tangent) is adopted to locate the inflection point.

| Lattice         | $\mu_{l,I}/(\pi T)$ | $\mu_{s,I}/(\pi T)$ | $T_c(\bar{\psi}\psi)$ | $T_c(\chi^r)$ |
|-----------------|---------------------|---------------------|-----------------------|---------------|
| $16^3 \times 6$ | 0.00                | 0.00                | 148.2(3)              | 150.7(4)      |
| $16^3 \times 6$ | 0.20                | 0.00                | 155.0(4)              | 157.0(4)      |
| $16^3 \times 6$ | 0.24                | 0.00                | 158.9(4)              | 160.0(4)      |
| $16^3 \times 6$ | 0.275               | 0.00                | 161.2(4)              | 162.7(4)      |
| $24^3 \times 6$ | 0.00                | 0.00                | 149.0(6)              | 151.6(5)      |
| $24^3 \times 6$ | 0.24                | 0.00                | 160.8(7)              | 162.0(5)      |
| $24^3 \times 6$ | 0.275               | 0.00                | 164.1(4)              | 165.9(4)      |
| $32^3 \times 6$ | 0.00                | 0.00                | 149.1(7)              | 152.0(4)      |
| $32^3 \times 6$ | 0.24                | 0.00                | 160.2(3)              | 162.7(4)      |
| $32^3 \times 6$ | 0.275               | 0.00                | 163.4(3)              | 165.5(4)      |
| $32^3 \times 8$ | 0.00                | 0.00                | 154.2(4)              | 155.6(7)      |
| $32^3 \times 8$ | 0.20                | 0.00                | 162.9(8)              | 163.0(6)      |
| $32^3 \times 8$ | 0.24                | 0.00                | 165.0(5)              | 165.8(8)      |
| $32^3 \times 8$ | 0.275               | 0.00                | 169.5(9)              | 169.8(7)      |
| $32^3 \times 8$ | 0.20                | 0.20                | 163.9(6)              | 165.3(9)      |
| $32^3 \times 8$ | 0.24                | 0.24                | 169.4(7)              | 169.6(7)      |
| $32^3 \times 8$ | 0.275               | 0.275               | 175.4(6)              | 177.0(8)      |

TABLE I: Critical temperatures obtained from the renormalized chiral condensate and from the renormalized chiral susceptibility. Reported errors do not take into account the uncertainty on the determination of the physical scale, which is of the order of 2-3 % [38, 39].

In the case of the renormalized chiral susceptibility, a reasonable description of the data around the peak location is provided by a Lorentzian function

$$\chi_{\psi\psi}^r = \frac{A_2}{B_2^2 + (T - T_c)^2}. \quad (20)$$

A fit to this function provides  $T_c$ , whose statistical error is again estimated by a bootstrap analysis. Finally, a systematic error is also taken into account and estimated by changing, for each data set, the fitted range of temperatures around the peak. In Fig. 5 we report numerical data for the dimensionless ratio  $\chi_{\psi\psi}^r/m_\pi^4$  as a function of  $T$ , together with some of the fits performed <sup>2</sup>.

The full set of determinations of  $T_c(\mu_{l,I}, \mu_{s,I})$  is reported in Table I. We stress that such values do not take into account the error on the determination of the physical scale, which is of the order of 2-3 % [38, 39]; on the other hand, since such error affects all  $T_c$  values in the same way, its effect on the ratio of pseudo-critical temperatures, which is the quantity entering the determination of  $\kappa$ , is expected to be negligible.

In order to extract the curvature, we performed a fit to the values obtained for  $T_c(\mu_{l,I})$ , separately for each lattice size and setup of chemical potentials, according

<sup>2</sup> Notice that if  $T$ -dependent dimensionless combinations of the susceptibility are adopted, like, e.g.,  $\chi_{\psi\psi}^r/T^4$ , the behavior deviates significantly from a Lorentzian function. Moreover, the locations of the maxima move to lower values of  $T$  by about 5 MeV.

to the function<sup>3</sup>

$$T_c(\mu_{l,I}) = T_c(0) \left( 1 + 9\kappa \left( \frac{\mu_{l,I}}{T_c(\mu_{l,I})} \right)^2 + 81b \left( \frac{\mu_{l,I}}{T_c(\mu_{l,I})} \right)^4 + O(\mu_{l,I}^6) \right). \quad (21)$$

In this way we got estimates of  $\kappa$  for all the lattices and the chemical potential setups adopted. The results of these fits are reported in Tables II and III, for the critical temperatures obtained from the chiral condensate and for the chiral susceptibility respectively. In Figs. 6 and 7 data for  $T_c(\mu_{l,I})$  are plotted together with the results of the aforementioned fits. In most cases, a simple linear fit (i.e. setting  $b = 0$ ) works quite well; just for the  $\mu_s = \mu_l$  setup (studied only on the  $32^3 \times 8$  lattice) the introduction of a quartic correction is necessary in order to obtain reasonable values of the  $\chi^2$  test. It is tempting to associate the enhancement of non-linear corrections in the  $\mu_s = \mu_l$  setup to the fact that, in this case, the Roberge-Weiss endpoint is closer to the  $\mu_l = 0$  axis, so that the associated critical behavior might have a stronger influence on the small  $\mu_l$  region.

| Lattice         | $\mu_s$ | $T_c(0)$ | $\kappa$   | $b$       | $\chi^2/n_{dof}$ |
|-----------------|---------|----------|------------|-----------|------------------|
| $16^3 \times 6$ | 0.00    | 148.2(3) | 0.0133(4)  | -         | 1.4              |
| $24^3 \times 6$ | 0.00    | 149.1(6) | 0.0150(7)  | -         | 0.17             |
| $32^3 \times 6$ | 0.00    | 149.2(7) | 0.0142(8)  | -         | 0.2              |
| $32^3 \times 8$ | 0.00    | 154.2(4) | 0.0142(7)  | -         | 1.2              |
| $32^3 \times 8$ | $\mu_l$ | 154.0(4) | 0.0200(6)  | -         | 2.5              |
| $32^3 \times 8$ | $\mu_l$ | 154.2(4) | 0.0149(24) | 0.0008(4) | 0.04             |

TABLE II: Parameters of the best fit to  $T_c(\mu_{l,I})$  from the renormalized chiral condensate according to Eq. (21). Blank fields indicate that the corresponding parameter has been set to zero in that fit.

| Lattice         | $\mu_s$ | $T_c(0)$ | $\kappa$   | $b$       | $\chi^2/n_{dof}$ |
|-----------------|---------|----------|------------|-----------|------------------|
| $16^3 \times 6$ | 0.00    | 150.7(4) | 0.0119(6)  | -         | 0.1              |
| $24^3 \times 6$ | 0.00    | 151.5(5) | 0.0140(7)  | -         | 0.7              |
| $32^3 \times 6$ | 0.00    | 152.1(3) | 0.0134(5)  | -         | 0.4              |
| $32^3 \times 8$ | 0.00    | 155.6(6) | 0.0134(9)  | -         | 0.2              |
| $32^3 \times 8$ | $\mu_l$ | 155.2(6) | 0.0196(10) | -         | 3.3              |
| $32^3 \times 8$ | $\mu_l$ | 155.6(7) | 0.012(3)   | 0.0010(5) | 1.2              |

TABLE III: The same as in Table II, but using the critical temperatures estimated from the maxima of the renormalized chiral susceptibility.

<sup>3</sup> Both  $\kappa$  and  $b$  are normalized as the coefficients that would appear in the expansion in terms of  $\mu_B$ ; this is the reason of the factors 9 and 81 appearing in Eq. (21). Notice also that, going to the fourth order expansion, one needs to specify what is the temperature appearing in the ratio  $\mu/T$ , as we have done in Eq. (21).

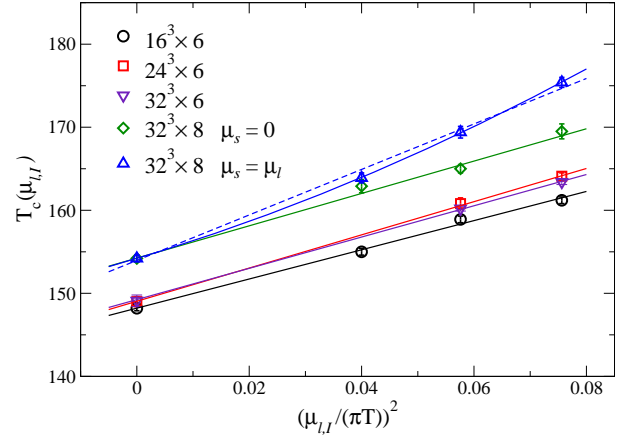


FIG. 6: Determinations of  $T_c$  obtained from the renormalized chiral condensate  $\langle \bar{\psi}\psi \rangle_l^r$  for various values of the chemical potential and lattice sizes. The lines correspond to quadratic and quartic fits in  $\mu_{l,I}$ , as discussed in the text. Fit results are reported in Table II.

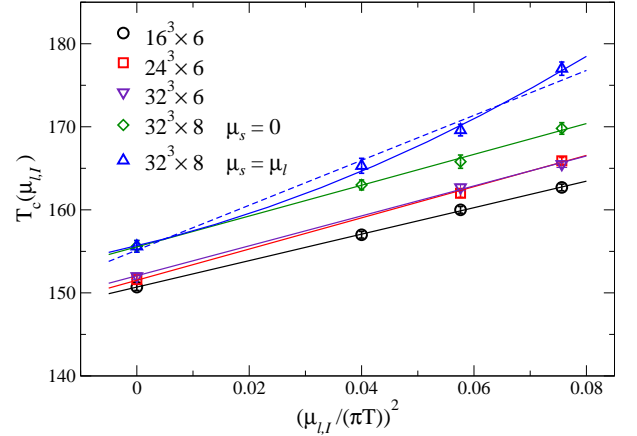


FIG. 7: Determinations of  $T_c$  obtained from the renormalized chiral susceptibility  $\chi_{\bar{\psi}\psi}^r$  for various values of the chemical potential and lattice sizes. The lines correspond to quadratic and quartic fits in  $\mu_{l,I}$ , as discussed in the text. Fit results are reported in Table III.

### A. Discussion of results

Let us now analyze the main features emerging from our results. A first important point is that, as one would expect, the value of  $T_c$  at zero chemical potential is in agreement with other existing determinations in the literature [1–5], i.e. in a range around 155 MeV.

Comparing data at the same lattice spacing and different spatial volumes ( $N_t = 6$  and  $L_s = 16, 24, 32$ ), or at the same physical spatial volume<sup>4</sup> and different lattice

<sup>4</sup> Lattices with the same aspect ratio  $L_s/N_t$  corresponds to approximately equal spatial volumes at the crossover, apart from



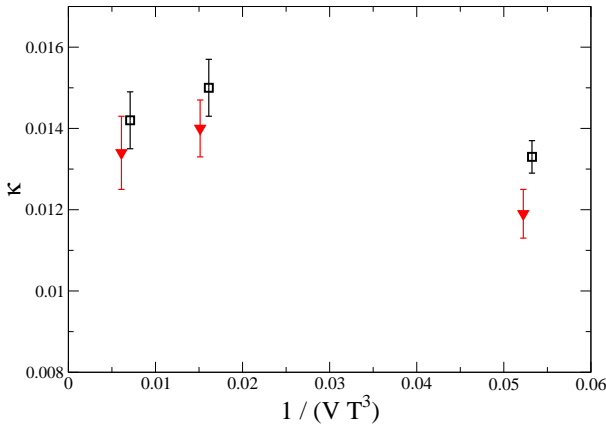


FIG. 8: Fitted values of the curvature  $\kappa$  from the  $N_t = 6$  lattices as a function of the inverse spatial volume. Squares correspond to the determinations obtained by using the chiral condensate, triangles to the chiral susceptibility estimates.

spacings ( $24^3 \times 6$  vs  $32^3 \times 8$ ), one concludes that both finite size and finite lattice spacing effects are visible in the determination of the pseudo-critical temperature at zero and nonzero  $\mu_l$ , both tending in general to decrease the value of  $T_c$ . It is also evident that the introduction of a non-zero  $\mu_{s,I} = \mu_{l,I}$  has a significant impact, leading to a relative temperature change  $T_c(\mu_{l,I})/T_c(0) - 1$  which is up to 40 % larger (at the largest value of  $\mu_{l,I}$  explored), with respect to the  $\mu_{s,I} = 0$  case.

On the other hand, when the dependence of  $T_c$  on  $\mu_{l,I}$  is considered, in order to extract the curvature, good part of these effects boils down to a constant shift of the curves or to the introduction of quartic corrections (see Figs. 6 and 7). That means, in particular, that the curvature  $\kappa$  is a more stable quantity: the introduction of the strange quark chemical potential does not modify it within present errors, finite lattice spacing effects seem to be within the 10 % level. Finite size effects are of the order of 15 % when going from lattices with aspect ratio  $\sim 2.7$  to lattices with aspect ratio 4. However they are much smaller and stay within statistical errors when going from aspect ratio 4 to aspect ratio  $\sim 5.3$ , suggesting that they are well under control already on lattices with aspect ratio 4; all that can be appreciated from Fig. 8, where we report our determinations of  $\kappa$  for  $N_t = 6$  and different spatial volumes.

In Fig. 9 we have reported our determinations of  $\kappa$  obtained for  $\mu_{s,I} = 0$  and on the lattices with aspect ratio 4, together with a rudimentary continuum extrapolation, performed assuming order  $a^2$  corrections. This cannot be considered as a rigorous continuum extrapolation yet, since we have not enough data points to perform a best fit. The numbers we obtain are  $\kappa = 0.0132(18)$  from the renormalized chiral condensate and  $\kappa = 0.0126(22)$  from

the renormalized chiral susceptibility, hence we have a very good agreement between the two determinations.

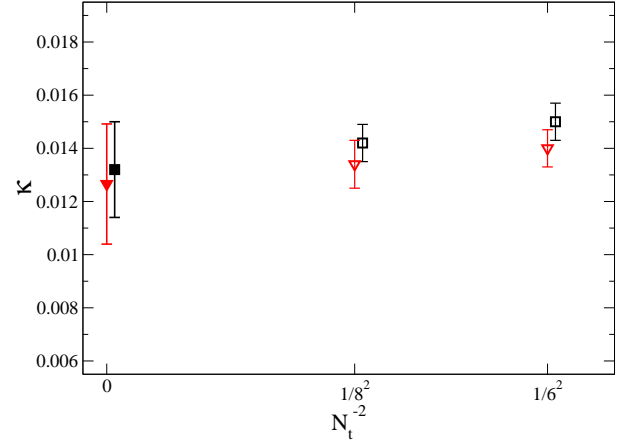


FIG. 9: Determinations of the critical line curvature  $\kappa$  as a function of  $N_t^{-2}$ . Squares correspond to the determinations obtained by using the chiral condensate, triangles to the chiral susceptibility estimates. The points at zero abscissa correspond to a rudimentary continuum limit extrapolation, assuming corrections linear in  $N_t^{-2}$ .

## V. COMPARISON WITH OTHER DETERMINATIONS

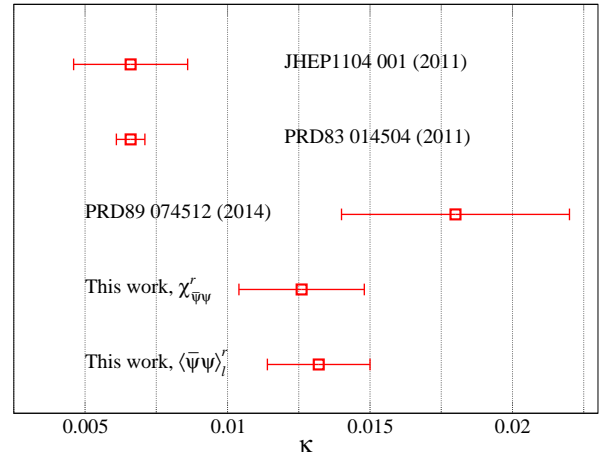


FIG. 10: Determinations of the critical line curvature  $\kappa$  in different works. From bottom to top: *i*) Analytic continuation, renormalized chiral condensate, this work; *ii*) Analytic continuation, renormalized chiral susceptibility, this work; *iii*) Analytic continuation, disconnected chiral susceptibility with  $\mu_s = \mu_l$ , Ref. [20]; *iv*) Taylor expansion, chiral susceptibility, Ref. [7]; *v*) Taylor expansion, chiral condensate (different renormalization), Ref. [8].

---

the residual  $a$ -dependence of  $T_c$ .

In Fig. 10 we compare our present results with previous ones in the literature. We do not report many early determinations and consider only a collection of recent

ones, which look at the chiral transition and have been obtained by discretizations of  $N_f = 2 + 1$  QCD at or close to the physical point [7, 8, 20]. Our results seem generally larger than results obtained by the Taylor expansion [7, 8] and in marginal agreement with results obtained by analytic continuation and a different discretization [20]. However, the correct assessment of possible discrepancies or agreement requires a careful analysis of the possible sources of systematic differences between the various determinations, a task that we try to accomplish in this Section.

Part of the effects are related to the different lattice discretizations adopted and should disappear as one approaches the continuum limit. Moreover, since no real transition takes place, the result depends on the particular physical quantity and on the prescription chosen to locate the crossover at zero and non-zero  $\mu_B$ . In this work, we have considered either the chiral condensate (renormalized as in Eq. (9)) and its inflection point, or the full chiral susceptibility (renormalized as in Eq. (13)) and its maximum: as we have already discussed, both are faithful, in the sense that provide a correct location of  $T_c$  in the case of a real transition.

The determination in Ref. [7] develops on previous studies carried on by the same group about the chiral transition at  $m_l = 0$  with physical  $m_s$  [56]. The basic idea is that, if for physical  $m_s$  the chiral transition is second order, the neighborhood of the critical point can be described by two scaling variables,  $t$  and  $h$ . To leading order only  $h$  depends on the chiral symmetry breaking parameter, *i.e.*  $m_l$ , and we thus have the relations

$$t \simeq \frac{1}{t_0} \left( \frac{T - T_c(0)}{T_c(0)} + \kappa \left( \frac{\mu_B}{T_c(0)} \right)^2 \right) \quad h \simeq \frac{1}{h_0} \frac{m_l}{m_s}, \quad (22)$$

where  $t_0$  and  $h_0$  are dimensionless factors. These can be fixed by imposing appropriate normalization conditions to the scaling functions (see [7, 56] for more details).

In Eq. (22) we denoted by  $T_c(0)$  the critical temperature at vanishing chemical potential and, since the transition for generic  $\mu_B$  is located at  $t = 0$ , it follows that  $\kappa$  is the curvature of the critical line as previously defined in Eq. (1). To extract the value of  $\kappa$  one can study an observable  $\varphi$  directly related to the critical behavior, like the chiral condensate, which plays a role analogous to the magnetization and, in the scaling regime, is governed by a well known scaling behavior  $\varphi \equiv \varphi(t, h)$ , which is fixed according to the  $O(4)$  universality class and was checked at  $\mu_B = 0$  in Ref. [56]. It is easy then to prove, by means of Eq. (22), that

$$\kappa = \frac{t_0}{\partial_t \varphi} \frac{\partial \varphi}{\partial (\mu_B/T)^2}. \quad (23)$$

In Ref. [7],  $\partial \varphi / \partial (\mu_B/T)^2$  was measured directly in terms of a mixed susceptibility computed at  $\mu_B = 0$ , while  $t_0 / \partial_t \varphi$  was fixed by the  $O(4)$  scaling function. In this way the value of  $\kappa$  was inferred by imposing a scaling behavior

for the mixed susceptibility computed for different values of the light quark mass.

In Ref. [19] a variant of this approach was proposed, which makes use of simulations performed at imaginary chemical potential (with  $\mu_l = \mu_s$ ). Having at disposal data obtained at  $\mu_B \neq 0$ , Eq. (22) can be used without the need of computing derivatives of observables: results are compatible with those of Ref. [7].

In this case, a direct comparison with our determination is not easy, since one has different lattice discretizations (p4 staggered action vs stout smeared staggered action) and no proper continuum extrapolation from both sides (Ref. [7] has lattices with  $N_t = 4, 8$ , Ref. [19] has lattices with  $N_t = 4$ ). Moreover, one should notice that the value of  $\kappa$  obtained in this way is actually the curvature of the second order line in the chiral limit  $m_l = 0$ , assuming  $O(4)$  critical behavior; the expectation is that the dependence of  $\kappa$  on the light quark mass is very mild.

A different procedure was put forward in Ref. [8]: for each observable  $\phi(T, \mu_B)$  that is monotonic in the neighborhood of the  $\mu_B = 0$  transition, the authors define the critical temperature at finite chemical potential (denoted by  $T_c(\mu_B)$ ) as the solution of the equation

$$\phi(T_c(\mu_B), \mu_B) = \phi(T_c(0), 0). \quad (24)$$

With this definition, along the  $(T_c(\mu_B), \mu_B)$  curve we have  $d\phi \equiv 0$ , thus we obtain

$$\begin{aligned} \kappa &\equiv -T_c(0) \left. \frac{dT_c(\mu_B)}{d\mu_B^2} \right|_{\mu_B=0} = \\ &= T_c(0) \left. \frac{\partial \phi / \partial \mu_B^2}{\partial \phi / \partial T} \right|_{\mu_B=0; T=T_c}. \end{aligned} \quad (25)$$

The strangeness susceptibility and the chiral condensate were used as the  $\phi$  observable in Ref. [8], with the following renormalization prescription for the chiral condensate:

$$\langle \bar{\psi} \psi \rangle_{(2)}^r = \frac{m_l}{m_\pi^4} (\langle \bar{\psi} \psi \rangle_l - \langle \bar{\psi} \psi \rangle_l(T=0)). \quad (26)$$

In Eq. (25), the derivative with respect to  $\mu_B^2$  is given in terms of a susceptibility computed at  $\mu_B = 0$ , as for Eq. (22), while  $\partial \phi / \partial T$  is obtained directly by numerical differentiation of data at various temperatures. Notice that this prescription for locating  $T_c$  might not be faithful in the particular case of a real transition and if the chosen observable is not an order parameter vanishing at  $T_c$ : indeed, in general, the value taken by the observable at  $T_c$  could change as the transition changes with  $\mu_B$ .

In this case, a detailed comparison with our determination makes sense, since we adopt the same lattice discretization and the same physical observable (chiral condensate), even if with a different renormalization prescription. In particular we can understand, making use of our data, what is the influence on the curvature of

adopting a different prescription for locating  $T_c$  and/or of adopting a different renormalization prescription for the chiral condensate (Eq. (9) vs Eq. (26)).

In Fig. 4 we can see that, if we use the inflection points (marked with filled triangles in the plots) as a definition of  $T_c(\mu_B)$ , Eq. (24) is only approximately satisfied, in particular at these points the condensate assumes values  $\langle\bar{\psi}\psi\rangle_l^T(T_c(\mu_{l,I}), \mu_{l,I})$  that decreases as  $\mu_{l,I}$  is increased. Therefore, adopting the prescription of Ref. [8] and defining  $T_c(\mu_{l,I})$  as the temperature for which the condensate takes the same value as for  $T_c(0)$ , we would obtain lower estimates of  $T_c(\mu_{l,I})$  and of  $\kappa$ . This is indeed what happens, as shown in Appendix B. Despite this consideration, however, the continuum extrapolated value of  $\kappa$  does not differ within the statistical errors.

A more substantial difference is obtained if, in addition, one also adopt the renormalization prescription of Ref. [8], i.e. Eq. (26) (see Appendix B for details). In this case our continuum extrapolated value would go from  $\kappa = 0.0132(18)$  to  $\kappa = 0.0110(18)$ , i.e. an effect of around 20%. Therefore, about one third of the discrepancy with respect to Ref. [8], claiming  $\kappa = 0.0066(20)$ , can be attributed to systematic effects connected to different prescriptions for renormalization or location of  $T_c$ : this is not unexpected, in view of the fact that there is no real phase transition in the range of chemical potentials under study. Taking that into account, the remaining discrepancy between the two determinations goes below 2 standard deviations. In the future, a more rigorous continuum extrapolation of our data could better clarify the issue.

Finally, we compare with the results published in Ref. [20], in which the authors adopt the method of analytic continuation, with the setup  $\mu_l = \mu_s$ , and locate  $T_c$  by looking for the maximum of the disconnected part of the unrenormalized chiral susceptibility. The outcome of such analysis is in marginal agreement with our determination. One should also take into account that, as illustrated in appendix B, adopting the unrenormalized disconnected susceptibility in place of the full renormalized one leads to an increased curvature: in our case the continuum extrapolated value goes from  $\kappa = 0.0126(22)$  to  $\kappa = 0.0146(41)$ , hence in better agreement with the outcome of Ref. [20]. That, taking into account that a different discretization was used in Ref. [20] (HISQ action), is compatible with the absence of significant lattice artifacts in both cases.

Regarding the different setup of chemical potentials, we have already verified on our results that the introduction of a non-zero  $\mu_s$  does not influence the value of  $\kappa$  significantly, but on the other hand it introduces larger non-linear corrections in  $\mu_{l,I}^2$ . In Ref. [20] there was no evidence of such non-linear corrections, even if only on the smallest lattice, namely  $16^3 \times 6$ , multiple values of  $\mu_{l,I}$  were explored.

## VI. CONCLUSIONS

We have presented a determination of the pseudo-critical line of  $N_f = 2 + 1$  QCD with physical quark masses by the method of analytic continuation from imaginary chemical potentials. We considered a stout smeared staggered discretization and performed simulations on lattices with  $N_t = 6$  and  $N_t = 8$ .

In order to locate the pseudo-critical temperature  $T_c$ , we have considered both the inflection point of the renormalized condensate or the location of the peak of the renormalized chiral susceptibility. The pseudo-critical temperature at zero quark chemical potential is found to be in agreement with previous determinations. Finite size effects on the curvature have been shown to be not significant, within present statistical errors, on lattices with aspect ratio 4. A preliminary continuum extrapolation of the curvature yields  $\kappa = 0.0132(18)$  for the chiral condensate and  $\kappa = 0.0126(22)$  for the chiral susceptibility.

This is in marginal agreement with recent results obtained by the method of analytic continuation [20], and larger than previous lattice determinations obtained by the Taylor expansion technique [7, 8] (notice however that larger values of the curvature have been obtained when considering different observables, like the strange quark number susceptibility or thermodynamical quantities [8, 9]). To better assess this issue, we have analyzed various possible systematic effects. Adopting the same conventions for renormalizing the chiral condensate and for locating  $T_c$  used in Ref. [8], our estimate from the condensate would go down to  $\kappa = 0.0110(18)$ ; hence, taking into account such systematics, the discrepancy with respect to results with the same lattice discretization appears to be below the  $2\sigma$  level. Adopting the disconnected chiral susceptibility in place of the full renormalized one, as in Ref. [20], our estimate from this observable would go up to  $\kappa = 0.0146(41)$ , in better agreement with Ref. [20].

We have also considered the effects of the introduction of a nonzero strange quark chemical potential  $\mu_s = \mu_l$ . The curvature stays unchanged within the present accuracy. This is reassuring for what concerns the comparison with the phenomenological conditions reproduced in heavy ion collisions: the requirement for strangeness neutrality corresponds, around the transition, to  $\mu_s/\mu_B \sim 1/4$  (see, e.g., Ref. [57]), hence to  $\mu_s \sim \mu_l/4$  (see Eq. (4)), i.e. a value of  $\mu_s$  which is in-between the two cases explored in our simulations. On the contrary, non-linear terms in  $\mu_l^2$  become larger for  $\mu_s = \mu_l$ . The origin of this difference could be related to the different phase structure which is found, for imaginary chemical potentials, at the different values of  $\mu_s$ . In particular, the so-called Roberge-Weiss line and the associated non-analytic behavior moves further from the  $\mu_l = 0$  axis when  $\mu_s = 0$ .

Given the agreement between the two determinations, obtained from the renormalized chiral condensate and from the renormalized chiral susceptibility, we quote

$\kappa = 0.013(2)(1)$  as our present estimate for the curvature of the chiral pseudo-critical line. The second error is an estimate of the residual systematic uncertainty on the cut-off effects, and is obtained by comparing with an extrapolation which assumes a flat behavior with  $N_t$ , which is also compatible with our present results. In the future we plan to extend our investigation to lattices with at least  $N_t = 10$ , in order to fully remove the systematics associated with the continuum extrapolation.

### Acknowledgments

We thank F. Becattini, L. Cosmai, G. Endrodi, P. de Forcrand, F. Karsch, M. P. Lombardo, A. Papa and A. Patella for useful discussions. FS received funding from the European Research Council under the European Communitys Seventh Framework Programme (FP7/2007-2013) ERC grant agreement No 279757. FN acknowledges financial support from the EU under project Hadron Physics 3 (Grant Agreement n. 283286). This work was partially supported by the INFN SUMA project. Simulations have been performed on the Blue-Gene/Q Fermi at CINECA (Project Iskra-B/EPDISIM), and on the CSN4 Zefiro cluster of the Scientific Computing Center at INFN-PISA.

### Appendix A: Parameter sets and data at $T = 0$

The determination of the renormalized observables used to locate  $T_c$  requires the computation of the chiral condensate and of the chiral susceptibility in the zero temperature limit and at the same UV cutoff (*i.e.* the same values of  $\beta$  and of the bare quark masses) of the finite temperature data. To that aim, we spanned a range of  $\beta$  on the line of constant physics,  $3.5 \leq \beta \leq 3.8$ , on a symmetric  $32^4$  lattice, corresponding to  $T$  in the range 25 – 55 MeV. We report the results for the condensate and for the susceptibility in Table IV.

The temperatures are low enough to be considered as a good approximation of the  $T = 0$  limit; indeed, as expected because of the absence of transitions in this  $T$  range, one observes a very smooth dependence of the observables on  $\beta$ . Hence, the relatively coarse sampling of the interval is enough to allow for a reliable interpolation. We adopted a cubic spline interpolation for the condensate and a linear fit for the susceptibility.

The renormalization prescription for the susceptibility that we adopted throughout the paper requires the subtraction of the  $T = 0$  result from the  $T \neq 0$  contribution. To give an idea of the relative magnitude of the two contributions, in Fig 11 we plot the chiral susceptibilities  $\chi_{\bar{\psi}\psi}$ , defined in Eq. (10), both at zero and at finite temperature, at zero chemical potential.

Finally, for completeness, we report in Table V the full set of bare parameters and lattice spacings adopted in our simulations, both at zero and non-zero  $T$ . Data have

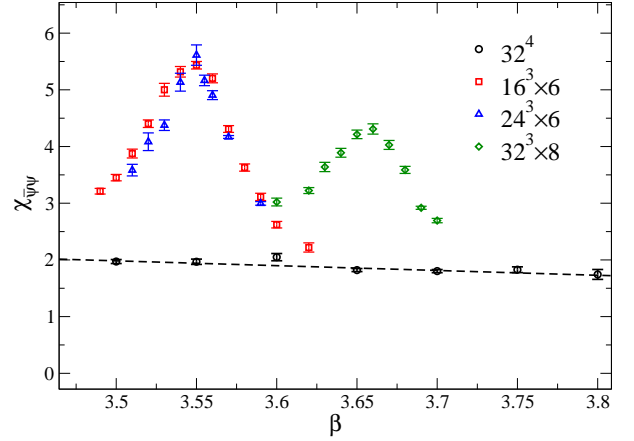


FIG. 11: Comparison between the zero and finite temperature chiral susceptibility at zero chemical potential. These terms are required to compute the renormalized chiral susceptibility, see Eq. (13). Data on the vertical axis are in lattice units. A linear fit of the  $T = 0$  data is also shown.

| $\beta$ | $\chi_{\bar{\psi}\psi}$ | $\langle\bar{\psi}\psi\rangle - 2(m_l/m_s)\langle\bar{s}s\rangle$ |
|---------|-------------------------|---|
| 3.50    | 1.972(35)               | 0.07999(11)   |
| 3.55    | 1.968(46)               | 0.05680(13)   |
| 3.60    | 2.049(64)               | 0.03912(14)   |
| 3.65    | 1.821(27)               | 0.02633(17)   |
| 3.70    | 1.803(28)               | 0.018041(3)   |
| 3.75    | 1.827(51)               | 0.01208(11)   |
| 3.80    | 1.744(88)               | 0.008348(7)   |

TABLE IV: Determination of the observables at  $T = 0$  (on the  $32^4$  lattice) needed to perform the renormalizations discussed in Section II. Data are in lattice units.

been determined by a spline interpolation of the values reported in Refs. [38, 39]. As a crosscheck, we have performed an independent determination of the pion mass on our zero temperature lattices, obtaining values in the range 133-137 MeV for the set of parameters explored: given the overall 2-3% systematic error on the determination of the lattice spacing, this is satisfactory.

### Appendix B: Comparison with other methods

In this Appendix we analyze how the determinations of  $T_c$  and  $\kappa$  change if different prescriptions are adopted to renormalize observables or to locate  $T_c$ .

Regarding the determination of  $\kappa$  from the chiral condensate we compare two different renormalization prescriptions of the condensate and two different methods to extract  $T_c$ . We set the following notation:  $C_1$  is the chiral condensate renormalized as in Eq. (9), while  $C_2$  is the one renormalized as in Eq. (26). For what concerns the method we define  $M_1$  as the determination of  $T_c$  obtained from the inflection point of  $\langle\bar{\psi}\psi\rangle_l^*$ , which is the one adopted in this work, and  $M_2$  as the determination based on Eq. (24); in the latter case, we have taken the



| $\beta$ | $L_s$    | $N_t$  | $m_s$   | $a[\text{fm}]$ |
|---------|----------|--------|---------|----------------|
| 3.490   | 16       | 6      | 0.132   | 0.2556         |
| 3.500   | 16,32    | 6,32   | 0.126   | 0.2490         |
| 3.510   | 16,24,32 | 6      | 0.121   | 0.2425         |
| 3.520   | 16,24,32 | 6      | 0.116   | 0.2361         |
| 3.530   | 16,24,32 | 6      | 0.111   | 0.2297         |
| 3.540   | 16,24,32 | 6      | 0.10643 | 0.2235         |
| 3.550   | 16,24,32 | 6,32   | 0.10200 | 0.2173         |
| 3.555   | 24       | 6      | 0.09987 | 0.2142         |
| 3.560   | 16,24,32 | 6      | 0.09779 | 0.2112         |
| 3.570   | 16,24,32 | 6      | 0.09378 | 0.2052         |
| 3.580   | 16,24,32 | 6      | 0.08998 | 0.1994         |
| 3.590   | 16,24,32 | 6      | 0.08638 | 0.1937         |
| 3.595   | 24       | 6      | 0.08465 | 0.1908         |
| 3.600   | 16,24,32 | 6,8,32 | 0.08296 | 0.1881         |
| 3.610   | 16,32    | 6      | 0.07973 | 0.1826         |
| 3.620   | 16,24,32 | 6,8    | 0.07668 | 0.1773         |
| 3.630   | 16,32    | 6,8    | 0.07381 | 0.1722         |
| 3.640   | 16,32    | 6,8    | 0.07110 | 0.1672         |
| 3.650   | 16,32    | 6,8,32 | 0.06854 | 0.1625         |
| 3.660   | 16,32    | 6,8    | 0.06615 | 0.1579         |
| 3.670   | 32       | 8      | 0.06390 | 0.1535         |
| 3.680   | 16,32    | 6,8    | 0.06179 | 0.1493         |
| 3.690   | 32       | 8      | 0.05982 | 0.1453         |
| 3.700   | 32       | 8,32   | 0.05797 | 0.1416         |
| 3.710   | 32       | 8      | 0.05624 | 0.1379         |
| 3.720   | 32       | 8      | 0.05462 | 0.1345         |
| 3.730   | 32       | 8      | 0.05309 | 0.1312         |
| 3.740   | 32       | 8      | 0.05166 | 0.1280         |
| 3.750   | 32       | 8,32   | 0.05030 | 0.1249         |
| 3.800   | 32       | 32     | 0.04445 | 0.1110         |

TABLE V: List of bare parameters and lattice spacings adopted in the simulations at zero and non-zero  $T$ ; the light quark mass is not reported, we have set  $m_l = m_s/28.15$  in all cases. For each set of bare parameters, we report the various spatial and temporal sizes adopted (notice that some possible combinations of  $L_s$  and  $N_t$  have not been used). The systematic error on the lattice spacing is of the order of 2-3 % [38, 39].

value of the condensate at the inflection point at zero chemical potential as the reference value which is kept constant at nonzero  $\mu_B$ .

According to these definitions, the method that we adopted throughout the paper can be addressed as  $C_1M_1$ . In Table VI we show the results for  $T_c$  obtained by taking all different combinations. As we did in Section IV, we compute the curvature of the pseudo-critical line by fitting the extracted values of  $T_c$  by Eq. (21). The results of these fits are reported in Table VII, VIII and IX respectively for the combinations  $C_1M_2$ ,  $C_2M_1$  and  $C_2M_2$ .

Regarding the determination of  $\kappa$  from the chiral susceptibility, in Table X we report the results for the pseudo-critical temperature as a function of the chemical potential obtained from the non-renormalized disconnected chiral susceptibility  $\chi_{\psi\psi}^{disc}$ , defined in Eq. (11). The disconnected susceptibility is measured in lattice spacing units: that leads to an additional  $T = 1/(N_t a)$  dependence, which can account for the generally lower values

| Lattice         | $\theta_l/\pi$ | $\theta_s/\pi$ | $C_1M_1$ | $C_1M_2$ | $C_2M_1$ | $C_2M_2$ |
|-----------------|----------------|----------------|----------|----------|----------|----------|
| $16^3 \times 6$ | 0.00           | 0.00           | 148.2(3) | 148.2(2) | 148.4(4) | 148.4(2) |
| $16^3 \times 6$ | 0.20           | 0.00           | 155.0(4) | 154.6(2) | 155.1(5) | 154.8(2) |
| $16^3 \times 6$ | 0.24           | 0.00           | 158.9(4) | 157.8(2) | 159.1(4) | 158.1(2) |
| $16^3 \times 6$ | 0.275          | 0.00           | 161.2(4) | 160.5(2) | 161.5(4) | 160.8(2) |
| $24^3 \times 6$ | 0.00           | 0.00           | 149.0(6) | 149.0(2) | 149.0(6) | 149.0(2) |
| $24^3 \times 6$ | 0.24           | 0.00           | 160.8(7) | 159.6(2) | 160.7(5) | 159.6(2) |
| $24^3 \times 6$ | 0.275          | 0.00           | 164.1(4) | 163.0(2) | 164.3(3) | 163.1(2) |
| $32^3 \times 6$ | 0.00           | 0.00           | 149.3(3) | 149.3(1) | 149.4(4) | 149.4(1) |
| $32^3 \times 6$ | 0.24           | 0.00           | 160.2(2) | 159.5(1) | 160.4(2) | 159.6(1) |
| $32^3 \times 6$ | 0.275          | 0.00           | 163.5(3) | 162.7(1) | 163.5(3) | 162.7(1) |
| $32^3 \times 8$ | 0.00           | 0.00           | 154.2(4) | 154.2(2) | 154.5(4) | 154.5(2) |
| $32^3 \times 8$ | 0.20           | 0.00           | 162.9(8) | 161.6(2) | 163.0(6) | 161.8(2) |
| $32^3 \times 8$ | 0.24           | 0.00           | 165.0(5) | 164.5(2) | 164.8(5) | 164.5(2) |
| $32^3 \times 8$ | 0.275          | 0.00           | 169.5(9) | 168.6(3) | 168.6(7) | 168.4(3) |
| $32^3 \times 8$ | 0.20           | 0.20           | 163.9(6) | 163.3(2) | 163.7(6) | 163.4(2) |
| $32^3 \times 8$ | 0.24           | 0.24           | 169.4(7) | 168.3(3) | 168.6(6) | 168.3(3) |
| $32^3 \times 8$ | 0.275          | 0.275          | 175.4(6) | 174.1(2) | 174.4(7) | 174.0(3) |

TABLE VI: Critical temperatures obtained by using different renormalization prescription and/or different definition of  $T_c$ , see text for symbol definitions.

| Lattice         | $\mu_s$ | Fit  | $T_c(0)$ | $\kappa$  | $b$       | $\chi^2/n_{dof}$ |
|-----------------|---------|------|----------|-----------|-----------|------------------|
| $16^3 \times 6$ | 0.00    | lin  | 148.2(2) | 0.0136(3) | -         | 0.8              |
| $24^3 \times 6$ | 0.00    | lin  | 149.0(2) | 0.0139(3) | -         | 0.2              |
| $32^3 \times 6$ | 0.00    | lin  | 149.3(1) | 0.0133(2) | -         | 0.1              |
| $32^3 \times 8$ | 0.00    | lin  | 154.2(2) | 0.0136(3) | -         | 2.5              |
| $32^3 \times 8$ | $\mu_l$ | lin  | 154.0(2) | 0.0187(3) | -         | 15.5             |
| $32^3 \times 8$ | $\mu_l$ | quad | 154.3(2) | 0.0137(9) | 0.0008(2) | 0.02             |

TABLE VII: Curvatures obtained by fitting the  $T_c$ s from the  $C_1M_2$  combination of Table VI.

of  $T_c$  obtained. Again, as we did in Section IV, we compute the curvature of the pseudo-critical line by fitting  $T_c$  with Eq. (21): we report the results in Table XI.

### Appendix C: One loop Polyakov effective potential

The effective potential for the Polyakov loop can be computed in perturbation theory, obtaining results valid in the limit of very high temperature. The effective potential can be written in term of the eigenvalues of the Polyakov loop, denoted by  $\lambda_j = e^{i\phi_j}$  (with  $\sum_j \phi_j = 0 \bmod 2\pi$ ). A one-loop computation in an  $SU(N_c)$  gauge theory coupled to  $N_f$  massless fermions gives (see, e.g., Ref. [42])

$$V_{\text{eff}} = \frac{\pi^2 T^4}{12} \left( \frac{1}{2} \sum_{j,k=1}^{N_c} V^{(g)}(j,k) - \sum_{f=1}^{N_f} \sum_{j=1}^{N_c} V^{(g)}(f,j) \right) \quad (\text{C1})$$

| Lattice         | $\mu_s$ | Fit  | $T_c(0)$ | $\kappa$   | $b$       | $\chi^2/n_{dof}$ |
|-----------------|---------|------|----------|------------|-----------|------------------|
| $16^3 \times 6$ | 0.00    | lin  | 148.5(3) | 0.0133(5)  | -         | 1.1              |
| $24^3 \times 6$ | 0.00    | lin  | 149.1(5) | 0.0152(7)  | -         | 0.0              |
| $32^3 \times 6$ | 0.00    | lin  | 149.5(3) | 0.0141(5)  | -         | 0.4              |
| $32^3 \times 8$ | 0.00    | lin  | 154.7(4) | 0.0135(7)  | -         | 2.5              |
| $32^3 \times 8$ | $\mu_l$ | lin  | 154.3(3) | 0.0186(5)  | -         | 4.5              |
| $32^3 \times 8$ | $\mu_l$ | quad | 154.3(3) | 0.0138(11) | 0.0008(3) | 0.0              |

TABLE VIII: Curvatures obtained by fitting the  $T_c$ s from the  $C_2M_1$  combination of Table VI.

| Lattice         | $\mu_s$ | Fit  | $T_c(0)$   | $\kappa$   | $b$       | $\chi^2/n_{dof}$ |
|-----------------|---------|------|------------|------------|-----------|------------------|
| $16^3 \times 6$ | 0.00    | lin  | 148.33(16) | 0.0124(3)  | -         | 12.5             |
| $24^3 \times 6$ | 0.00    | lin  | 148.49(23) | 0.0147(3)  | -         | 0.0              |
| $32^3 \times 6$ | 0.00    | lin  | 149.4(1)   | 0.0133(2)  | -         | 0.0              |
| $32^3 \times 8$ | 0.00    | lin  | 154.55(17) | 0.0131(3)  | -         | 1.7              |
| $32^3 \times 8$ | $\mu_l$ | lin  | 154.23(18) | 0.0181(3)  | -         | 14.6             |
| $32^3 \times 6$ | $\mu_l$ | quad | 154.56(19) | 0.0133(10) | 0.0006(8) | 0.0              |

TABLE IX: Curvatures obtained by fitting the  $T_c$ s from the  $C_2M_2$  combination (*i.e.* the same method adopted in Ref. [8]) of Table VI.

| Lattice         | $\theta_l/\pi$ | $\theta_s/\pi$ | $T_c(\chi^r)$ | $T_c(\chi_{disc})$ |
|-----------------|----------------|----------------|---------------|--------------------|
| $16^3 \times 6$ | 0.00           | 0.00           | 150.7(4)      | 145.8(7)           |
| $16^3 \times 6$ | 0.20           | 0.00           | 157.0(4)      | 151.9(9)           |
| $16^3 \times 6$ | 0.24           | 0.00           | 160.0(4)      | 155.6(9)           |
| $16^3 \times 6$ | 0.275          | 0.00           | 162.7(4)      | 158.0(7)           |
| $24^3 \times 6$ | 0.00           | 0.00           | 151.6(5)      | 148.0(1.0)         |
| $24^3 \times 6$ | 0.24           | 0.00           | 162.0(5)      | 158.3(8)           |
| $24^3 \times 6$ | 0.275          | 0.00           | 165.9(4)      | 162.2(9)           |
| $32^3 \times 6$ | 0.00           | 0.00           | 152.0(4)      | 147.2(1.0)         |
| $32^3 \times 6$ | 0.24           | 0.00           | 162.7(4)      | 156.9(9)           |
| $32^3 \times 6$ | 0.275          | 0.00           | 165.5(4)      | 161.5(1.3)         |
| $32^3 \times 8$ | 0.00           | 0.00           | 155.6(7)      | 151.2(1.2)         |
| $32^3 \times 8$ | 0.20           | 0.00           | 163.0(6)      | 157.2(1.0)         |
| $32^3 \times 8$ | 0.24           | 0.00           | 165.8(8)      | 160.4(1.4)         |
| $32^3 \times 8$ | 0.275          | 0.00           | 169.8(7)      | 166.1(1.3)         |
| $32^3 \times 8$ | 0.20           | 0.20           | 165.3(9)      | 159.3(9)           |
| $32^3 \times 8$ | 0.24           | 0.24           | 169.6(7)      | 164.8(1.5)         |
| $32^3 \times 8$ | 0.275          | 0.275          | 177.0(8)      | 172.9(1.3)         |

TABLE X: Critical temperatures obtained from the non-renormalized disconnected chiral susceptibility. The values obtained from  $\chi^r$  are reported for reference.

| Lattice         | $\mu_s$ | Fit  | $T_c(0)$   | $\kappa$   | $b$       | $\chi^2/n_{dof}$ |
|-----------------|---------|------|------------|------------|-----------|------------------|
| $16^3 \times 6$ | 0.00    | lin  | 145.8(7)   | 0.0126(10) | -         | 0.2              |
| $24^3 \times 6$ | 0.00    | lin  | 147.9(1.0) | 0.0141(13) | -         | 0.2              |
| $32^3 \times 6$ | 0.00    | lin  | 147.0(1.0) | 0.0138(16) | -         | 0.8              |
| $32^3 \times 8$ | 0.00    | lin  | 150.5(1.1) | 0.0143(17) | -         | 1.3              |
| $32^3 \times 8$ | $\mu_l$ | lin  | 149.8(1.1) | 0.0208(18) | -         | 3.8              |
| $32^3 \times 8$ | $\mu_l$ | quad | 151.2(1.2) | 0.008(5)   | 0.0020(7) | 0.04             |

TABLE XI: Curvatures extracted from the data of Table X.

where  $V^{(g)}$  and  $V^{(q)}$  are the gluon and quark contributions respectively, explicitly given by

$$\begin{aligned}
 V^{(g)}(j, k) &= \left( 1 - \left( \left[ \frac{\phi_j}{\pi} - \frac{\phi_k}{\pi} \right]_{\text{mod } 2} - 1 \right)^2 \right)^2 \\
 V^{(q)}(f, j) &= \left( 1 - \left( \left[ \frac{\phi_j + \theta_f}{\pi} + 1 \right]_{\text{mod } 2} - 1 \right)^2 \right)^2.
 \end{aligned} \tag{C2}$$

In the expression for  $V^{(q)}$ ,  $\theta_f = \text{Im}(\mu_f)/T$  is the angle introduced in Section II, associated with the chemical potential of the quark flavor  $f$ .

For  $SU(3)$  pure gauge theory the minima of  $V_{\text{eff}}$  are degenerate and located on the cubic roots of the identity, *i.e.*  $\phi_j = \frac{2\pi}{3}k \forall j$ , where  $k = 0, 1, 2$ . Fermions lift this degeneracy: the cubic roots are still local minima but they are not degenerate any more; in the case of three flavors having the same chemical potential (*i.e.*  $\mu_u = \mu_d = \mu_s$ ), the absolute minimum changes by increasing  $\theta$ , with transitions taking place at  $\theta_c = (2n+1)\pi/3$ , where  $n$  is an integer.

As noted in Section III, one expects the position of these transitions to change when  $\mu_u = \mu_d$  but  $\mu_s = 0$ . This can be explicitly seen by using Eq. (C1). The potential evaluated on the three cubic roots of the identity is plotted in Fig. 12: the level crossings (corresponding to sector changes) move with respect to the  $\mu_l = \mu_s$  setup, the first one being located at  $\theta_c \approx 0.482933\pi$ . For comparison, we report also the analysis for the standard RW case ( $\mu_s = \mu_u = \mu_d$ ) in Fig. 13.

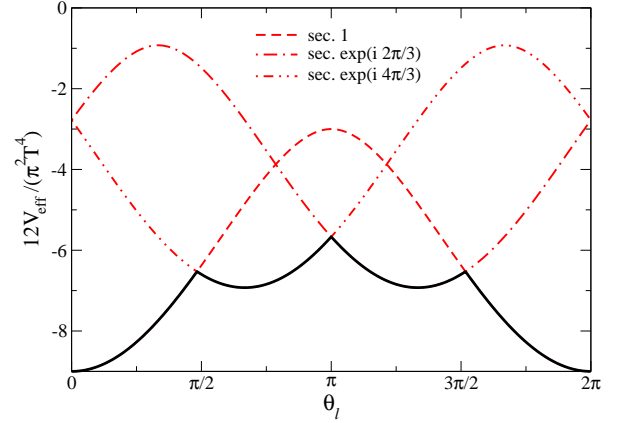


FIG. 12: Effective Polyakov loop potential computed from Eq. (C1) for  $\mu_u = \mu_d$  and  $\mu_s = 0$ .

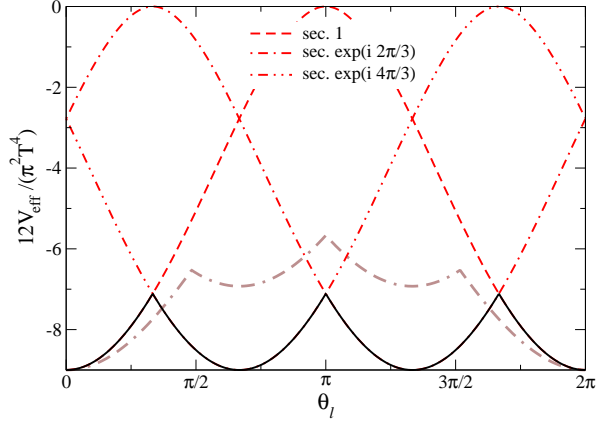


FIG. 13: Same as in Fig. 12, but for  $\mu_s = \mu_u = \mu_d$ : this is actually the same as Fig. 2 of Ref. [42]. The true vacuum potential from Fig. 12 is also reported to allow for a direct comparison of the two cases.

- 
- [1] Y. Aoki, G. Endrodi, Z. Fodor, S. D. Katz and K. K. Szabo, *Nature* **443** (2006) 675 [hep-lat/0611014].
- [2] Y. Aoki, Z. Fodor, S. D. Katz and K. K. Szabo, *Phys. Lett. B* **643**, 46 (2006) [hep-lat/0609068].
- [3] S. Borsanyi *et al.*, *JHEP* **1009**, 073 (2010).
- [4] A. Bazavov, T. Bhattacharya, M. Cheng, C. DeTar, H. T. Ding, S. Gottlieb, R. Gupta and P. Hegde *et al.*, *Phys. Rev. D* **85**, 054503 (2012) [arXiv:1111.1710 [hep-lat]].
- [5] T. Bhattacharya, M. I. Buchoff, N. H. Christ, H. -T. Ding, R. Gupta, C. Jung, F. Karsch and Z. Lin *et al.*, arXiv:1402.5175 [hep-lat].
- [6] C. R. Allton, S. Ejiri, S. J. Hands, O. Kaczmarek, F. Karsch, E. Laermann, C. Schmidt and L. Scorzato, *Phys. Rev. D* **66**, 074507 (2002) [hep-lat/0204010].
- [7] O. Kaczmarek, F. Karsch, E. Laermann, C. Miao, S. Mukherjee, P. Petreczky, C. Schmidt, W. Soeldner and W. Unger, *Phys. Rev. D* **83**, 014504 (2011) [arXiv:1011.3130 [hep-lat]].
- [8] G. Endrodi, Z. Fodor, S. D. Katz and K. K. Szabo, *JHEP* **1104**, 001 (2011) [arXiv:1102.1356 [hep-lat]].
- [9] S. Borsanyi, G. Endrodi, Z. Fodor, S. D. Katz, S. Krieg, C. Ratti and K. K. Szabo, *JHEP* **1208**, 053 (2012) [arXiv:1204.6710 [hep-lat]].
- [10] P. de Forcrand and O. Philipsen, *Nucl. Phys. B* **642**, 290 (2002) [hep-lat/0205016]; *Nucl. Phys. B* **673**, 170 (2003) [hep-lat/0307020].
- [11] M. D'Elia and M. P. Lombardo, *Phys. Rev. D* **67**, 014505 (2003) [hep-lat/0209146]; *Phys. Rev. D* **70**, 074509 (2004) [hep-lat/0406012].
- [12] V. Azcoiti, G. Di Carlo, A. Galante and V. Laliena, *Nucl. Phys. B* **723**, 77 (2005) [hep-lat/0503010].
- [13] L. K. Wu, X. Q. Luo and H. S. Chen, *Phys. Rev. D* **76**, 034505 (2007) [hep-lat/0611035].
- [14] P. Cea, L. Cosmai, M. D'Elia and A. Papa, *Phys. Rev. D* **77**, 051501 (2008) [arXiv:0712.3755 [hep-lat]].
- [15] P. Cea, L. Cosmai, M. D'Elia, C. Manneschi and A. Papa, *Phys. Rev. D* **80**, 034501 (2009) [arXiv:0905.1292 [hep-lat]].
- [16] P. Cea, L. Cosmai, M. D'Elia and A. Papa, *Phys. Rev. D* **81**, 094502 (2010) [arXiv:1004.0184 [hep-lat]].
- [17] K. Nagata and A. Nakamura, *Phys. Rev. D* **83**, 114507 (2011) [arXiv:1104.2142 [hep-lat]].
- [18] P. Cea, L. Cosmai, M. D'Elia, A. Papa and F. Sanfilippo, *Phys. Rev. D* **85**, 094512 (2012) [arXiv:1202.5700 [hep-lat]].
- [19] E. Laermann, F. Meyer and M. P. Lombardo, *J. Phys. Conf. Ser.* **432**, 012016 (2013). E. Laermann, F. Meyer and M. P. Lombardo, arXiv:1304.3247 [hep-lat].
- [20] P. Cea, L. Cosmai and A. Papa, *Phys. Rev. D* **89**, 074512 (2014) [arXiv:1403.0821 [hep-lat]].
- [21] Z. Fodor and S. D. Katz, *JHEP* **0203**, 014 (2002) [hep-lat/0106002].
- [22] Z. Fodor and S. D. Katz, *JHEP* **0404**, 050 (2004) [hep-lat/0402006].
- [23] S. Kratochvila and P. de Forcrand, *PoS LAT* **2005**, 167 (2006) [hep-lat/0509143].
- [24] A. Alexandru, M. Faber, I. Horvath and K. F. Liu, *Phys. Rev. D* **72**, 114513 (2005) [hep-lat/0507020].
- [25] P. Braun-Munzinger, J. Stachel, J. P. Wessels and N. Xu, *Phys. Lett. B* **344**, 43 (1995) [nucl-th/9410026]; *Phys. Lett. B* **365**, 1 (1996) [nucl-th/9508020].
- [26] F. Becattini, *Z. Phys. C* **69**, 485 (1996).
- [27] F. Becattini and U. W. Heinz, *Z. Phys. C* **76**, 269 (1997) [Erratum-ibid. *C* **76**, 578 (1997)] [hep-ph/9702274].
- [28] F. Becattini, J. Cleymans, A. Keranen, E. Suhonen and K. Redlich, *Phys. Rev. C* **64**, 024901 (2001) [hep-ph/0002267].
- [29] P. Braun-Munzinger, D. Magestro, K. Redlich and J. Stachel, *Phys. Lett. B* **518**, 41 (2001) [hep-ph/0105229].
- [30] A. Andronic, P. Braun-Munzinger and J. Stachel, *Nucl. Phys. A* **772**, 167 (2006) [nucl-th/0511071].
- [31] J. Cleymans, H. Oeschler, K. Redlich and S. Wheaton, *Phys. Rev. C* **73**, 034905 (2006) [hep-ph/0511094].
- [32] F. Becattini, M. Bleicher, T. Kollegger, T. Schuster,

- J. Steinheimer and R. Stock, Phys. Rev. Lett. **111**, 082302 (2013) [arXiv:1212.2431 [nucl-th]].
- [33] P. Weisz, Nucl. Phys. B **212**, 1 (1983).
- [34] G. Curci, P. Menotti and G. Paffuti, Phys. Lett. B **130**, 205 (1983) [Erratum-ibid. B **135**, 516 (1984)].
- [35] C. Morningstar and M. J. Peardon, Phys. Rev. D **69**, 054501 (2004) [hep-lat/0311018].
- [36] A. Bazavov *et al.* [HotQCD Collaboration], PoS LATTICE **2010**, 169 (2010) [arXiv:1012.1257 [hep-lat]].
- [37] A. Bazavov, D. Toussaint, C. Bernard, J. Laiho, C. DeTar, L. Levkova, M. B. Oktay and S. Gottlieb *et al.*, Rev. Mod. Phys. **82**, 1349 (2010) [arXiv:0903.3598 [hep-lat]].
- [38] Y. Aoki, S. Borsanyi, S. Durr, Z. Fodor, S. D. Katz, S. Krieg and K. K. Szabo, JHEP **0906**, 088 (2009) [arXiv:0903.4155 [hep-lat]].
- [39] S. Borsanyi, G. Endrodi, Z. Fodor, A. Jakovac, S. D. Katz, S. Krieg, C. Ratti and K. K. Szabo, JHEP **1011**, 077 (2010) [arXiv:1007.2580 [hep-lat]]; S. Borsanyi, Z. Fodor, C. Hoelbling, S. D. Katz, S. Krieg and K. K. Szabo, Phys. Lett. B **730**, 99 (2014) [arXiv:1309.5258 [hep-lat]].
- [40] M. Cheng, N. H. Christ, S. Datta, J. van der Heide, C. Jung, F. Karsch, O. Kaczmarek and E. Laermann *et al.*, Phys. Rev. D **77**, 014511 (2008) [arXiv:0710.0354 [hep-lat]].
- [41] M. D'Elia and F. Sanfilippo, Phys. Rev. D **80**, 014502 (2009) [arXiv:0904.1400 [hep-lat]].
- [42] A. Roberge and N. Weiss, Nucl. Phys. B **275** (1986) 734.
- [43] M. D'Elia, F. Di Renzo and M. P. Lombardo, Phys. Rev. D **76**, 114509 (2007) [arXiv:0705.3814 [hep-lat]].
- [44] C. Bonati and M. D'Elia, Phys. Rev. D **82**, 114515 (2010) [arXiv:1010.3639 [hep-lat]].
- [45] M. D'Elia and F. Sanfilippo, Phys. Rev. D **80**, 111501 (2009) [arXiv:0909.0254 [hep-lat]].
- [46] P. de Forcrand and O. Philipsen, Phys. Rev. Lett. **105**, 152001 (2010) [arXiv:1004.3144 [hep-lat]].
- [47] C. Bonati, G. Cossu, M. D'Elia and F. Sanfilippo, Phys. Rev. D **83**, 054505 (2011) [arXiv:1011.4515 [hep-lat]].
- [48] O. Philipsen and C. Pinke, Phys. Rev. D **89**, 094504 (2014) [arXiv:1402.0838 [hep-lat]].
- [49] K. Nagata and A. Nakamura, Phys. Rev. D **83**, 114507 (2011) [arXiv:1104.2142 [hep-lat]].
- [50] A. Alexandru and A. Li, PoS LATTICE **2013**, 208 (2013) [arXiv:1312.1201 [hep-lat]].
- [51] L.-K. Wu and X.-F. Meng, Phys. Rev. D **87**, 094508 (2013) [arXiv:1303.0336 [hep-lat]]; arXiv:1405.2425 [hep-lat].
- [52] K. Nagata, K. Kashiwa, A. Nakamura and S. M. Nishigaki, arXiv:1410.0783 [hep-lat].
- [53] M. A. Clark, A. D. Kennedy and Z. Sroczynski, Nucl. Phys. Proc. Suppl. **140**, 835 (2005) [hep-lat/0409133].
- [54] M. A. Clark and A. D. Kennedy, Phys. Rev. D **75**, 011502 (2007) [hep-lat/0610047].
- [55] M. A. Clark and A. D. Kennedy, Phys. Rev. Lett. **98**, 051601 (2007) [hep-lat/0608015].
- [56] S. Ejiri, F. Karsch, E. Laermann, C. Miao, S. Mukherjee, P. Petreczky, C. Schmidt, W. Soeldner and W. Unger, Phys. Rev. D **80**, 094505 (2009) [arXiv:0909.5122 [hep-lat]].
- [57] A. Bazavov, H.-T. Ding, P. Hegde, O. Kaczmarek, F. Karsch, E. Laermann, Y. Maezawa and S. Mukherjee *et al.*, Phys. Rev. Lett. **113**, 072001 (2014) [arXiv:1404.6511 [hep-lat]].